Homodinuclear lanthanide 9-anthracenecarboxylate complexes: Field induced SMM and NIR-luminescence

Berta Casanovas [a], Saskia Speed [a,b], Olivier Maury [b], Mercè Font-Bardía [c], Ramon Vicente [a,*]

a Departament de Química Inorgànica i Orgànica, Secció de Química Inorgànica, Universitat de Barcelona, Martí i Franquès 1-11, 08028 Barcelona, Spain
b Univ. de Lyon, UMR 5182–CNRS–Ecole Normale Supérieure de Lyon, Universtité de Lyon 1, 46 allée d'Italie, 69007 Lyon, France
c Departament de Mineralogia, Cristallografia i Dipòsits Minerals and Unitat de Difracció de R-X, Centres Científics i Tecnològics de la Universitat de Barcelona (CCiTUB), Universitat de Barcelona, Solé i Sabarís 1-3, 08028 Barcelona, Spain

rvicente@ub.edu (R. Vicente).

ABSTRACT:

Six homodinuclear lanthanide complexes with formula [Ln2(l2-9-AC)4(9-AC)2(phen)2] (Ln(III) = Nd (1), Eu (2), Gd (3), Tb (4), Er (5) and Yb (6) are reported and complexes 1–3 and 6 are structurally characterized. 9-HAC = 9-anthracenecarboxylic acid, phen = 1,10-phenanthroline. The luminescence properties of compounds 1–6 have been studied at different temperatures in the solid state and show the sensitization of the 4f–4f emission bands in the NIR range for compounds 1, 5 and 6. The molar magnetic susceptibility measurements of 1–6 in the 2–300 K temperature range indicate weak antiferromagnetic exchange for the isotropic Gd(III) compound 3. Furthermore, slow relaxation of the magnetization is found in complexes 5 and 6 with effective energy barriers of 9.5 cm 1 (0.1 T) and 22.7 cm 1 (0.15 T), respectively.

1. INTRODUCTION

Coordination compounds with lanthanide ions as central atoms are currently of great interest for the syntheses of novel molecular materials with interesting magnetic and luminescent properties [1–3]. From a magnetic point of view Ln(III) ions are ideal candidates to form complexes that could behave as single-molecule magnets (SMMs) [4] as they show an unquenched orbital angular momentum and significant spin–orbit coupling that yield large magnetic anisotropy and large magnetic moments in the ground state [5]. SMMs are molecules that present slow relaxation of the magnetization and have potential applications in quantum computing [6], high density data storage [7], and spintronics [8]. The energy barrier (Ea) that prevents the spin reversal in SMM compounds is proportional to the local anisotropy of the Ln(III) ions [9]. The existence of the strong spin–orbit coupling makes the magnetic anisotropy of lanthanide ions extremely sensitive to the shape and nature of the electrostatic ligand field around the ion [5].

Concerning the luminescence properties, the efficiently shielded electronic configuration of lanthanide ions confers them characteristic narrow f–f luminescence emission bands, long emission lifetimes, and large Stokes shifts. Unfortunately these f–f transitions are Laporte-forbidden and thus the compounds show low extinction coefficients needing to be indirectly excited by energy transfer processes from organic ligands or ‘‘antennas” that possess large extinction coefficients (e) [10,11]. Lanthanide ions emit in a wide range of wavelength from the UV–Vis to the NIR, and complexes emitting in the NIR region (e.g. Nd(III), Er(III), Yb(III)) are of great interest for optical communications [12], and for biological and sensor applications [10].

In order to isolate discrete 4f-metal ion complexes such as dinuclear entities, a successful synthetic approach to follow is the simultaneous employment of bidentate bridging anionic groups and chelating neutral capping organic ligands. For the anionic species, carboxylate ligands have been widely used due to the ability of carboxylate groups to interact with the Ln(III) ions [13–16]. As mentioned above, NIR emitting lanthanides are of great interest for several applications, and the anionic derivative of the 9-anthracenecarboxylic acid (9-HAC) can act as an efficient antenna for the sensitization of such Ln(III) ions [17–19]. On the other hand, chelating ligands may block two or three coordination sites of the Ln(III) ion, preventing further potential polymerization [20]. For this purpose, N-donor species such as 2,20-bipyridine (bpy), 1,10-phenanthroline (phen) or 2,20:60,200-terpyridine (terpy) are ideal candidates [21–28].

The synthesis of molecular complexes displaying simultaneously photoluminescence and SMM properties is a current interesting research field due to the potential applications of these systems in information storage, sensing and bioimaging [29,30]. Considering the aspects stated above and with the aim of obtaining multifunctional complexes displaying magnetic and luminescent properties, we have recently synthesised dinuclear lanthanide(III) complexes presenting both photoluminescence and field induced slow relaxation of the magnetisation by using 9-HAC and 2,20-bipyridine (bpy) ligands with

general formula [Ln2(l2-9-AC)4 (9-AC)2(bpy)2] [27]. Previously, Zhang, Liu and coworkers published the analogous SMM dysprosium [Dy2(l2-9-AC)4(9-AC)2(phen)2] compound in order to study the magnetic dependence on the variation of the chelating N-donor ligand [22].

Thus, with the aim of expanding these previous works herein we present the structure of four new dinuclear 4f-metal complexes synthesized using 9-HAC and the chelating 1,10-phenanthroline (phen) ligand. The new structurally reported compounds have the formula [Ln2(l2-9-AC)4(9-AC)2(phen)2] (where Ln(III) = Nd (1), Eu (2), Gd (3) and Yb (6)) which are isostructural to the previously reported Tb (4) [31] and Er (5) [32] compounds. The coordination number of the lanthanide ions is 9 for complexes 1–6. For the new compounds 1–3 and 6, we report here the syntheses, crystal structure, magnetic behaviour, and luminescence properties. For the previously published compounds 4 and 5, as only the structure was reported, we report also their magnetic and luminescent properties.

2. RESULTS AND DISCUSSION

2.1. Starting materials

Ln(NO3)3 6H2O salts (Strem Chemicals), 9-anthracenecarboxylic acid (TCI), 1,10-phenantholine and pyridine (Aldrich) were used as received without further purification.

2.2. Physical measurements

The elemental analyses of the compounds were performed at the Centres Científics i Tecnològics of the Universitat de Barcelona. Infrared spectra (4000–400 cm 1) were recorded from KBr pellets on a Perkin-Elmer 380-B spectrophotometer. The luminescence spectra were measured using a Horiba-Jobin Yvon Fluorolog-3 spectrofluorimeter, equipped with a three slit double grating excitation and emission monochromator with dispersions of 2.1 nm/mm (1200 grooves/mm). The steady-state luminescence was excited by unpolarized light from a 450Wxenon CW lamp and detected at an angle of 90 for diluted solution measurements and for solid state measurement by a red-sensitive Hamamatsu R928 photomultiplier tube. Spectra were reference corrected for both the excitation source light intensity variation (lamp and grating) and the emission spectral response (detector and grating). Near infra-red spectra were recorded at an angle of 90 using a liquid nitrogen cooled, solid indium/gallium/arsenic detector (850–1600 nm).

Magnetic measurements were performed on solid polycrystalline samples in a Quantum Design MPMS-XL SQUID magnetometer at the Magnetic Measurements Unit of the Universitat de Barcelona. Pascal's constants were used to estimate the diamagnetic corrections, which were subtracted from the experimental susceptibilities to give the corrected molar magnetic susceptibilities.

2.3. X-ray crystallography

Crystals of 1–3 and 6 were mounted in air on a Bruker APEX II CCD diffractometer. The crystallographic data, conditions retained for the intensity data collection and some features of the structure refinements are listed in Table S1. All the structures were refined by the least-squares method. Intensities were collected with a multilayer monochromated Mo Ka radiation. Lorentz polarization and absorption corrections were made in all the samples. The structures were solved by direct methods, using the SHELXS-97 computer program [33] and refined by full-matrix least-squares method, using the SHELXL-2014 computer program [34]. The nonhydrogen atoms were located in successive difference Fourier syntheses and refined with anisotropic thermal parameters on F2. For hydrogen atoms, isotropic temperature factors have been assigned as 1.2 or 1.5 times of the respective parent.

140 2.4. Syntheses
141 The dinuclear lanthanide complexes 1–6 were obtained based on the previously proposed synthetic
142 procedure for the [La2(l2-9-AC)4(9-AC)2(bpy)2] compound [35]. A mixture of 0.05 mmol of 9-
143 anthracenecarboxylic acid and 0.05 mmol of 1,10-phenanthroline in the presence of 0.05 mL of pyridine
144 in 10 mL of methanol is slowly diffused in a test tube with a solution of 0.1 mmol of the corresponding
145 Ln(NO3)3 nH2O salt in 15 mL of water. Yellow single crystals suitable for X-ray analysis of the
146 complexes appeared after a few days. The already published complexes 4 and 5 were characterized by
147 IR comparison (Fig. S1 in S1).
148 Anal. Calc. (%) for 1 (Nd) C, 69.28; H, 3.57; N, 2.83. Found: C, 68.8; H, 3.8; N, 2.9. Selected IR bands
149 (KBr pellet, cm 1): 1595 (vs), 1587 (vs), 1566 (s), 1513 (s), 1483 (m), 1425 (m), 1388 (s). (Yield:
150 0.030 g, 30% on the basis of Nd). Anal. Calc. (%) for 2 (Eu) C, 68.75; H, 3.54; N, 2.81. Found: C, 68.2;
151 H, 3.7; N, 2.9. Selected IR bands (KBr pellet, cm 1): 1598 (vs), 1589 (vs), 1569 (m), 1515 (s), 1487
152 (m), 1432 (s), 1388 (s). (Yield: 0.035 g, 35% on the basis of Eu). Anal. Calc. (%) for 3 (Gd) C, 68.38; H,
153 3.52; N, 2.80. Found: C, 67.1; H, 3.7; N, 2.9. Selected IR bands (KBr pellet, cm 1): 1597 (vs), 1582
154 (vs), 1576 (m), 1516 (s), 1487 (s), 1436 (s), 1388 (s). (Yield: 0.022 g, 22% on the basis of Gd). Anal.
155 Calc. (%) for 6 (Yb) C, 67.32; H, 3.47; N, 2.75. Found: C, 67.6; H, 3.6; N, 2.8. Selected IR bands (KBr
156 pellet, cm 1): 1606 (vs), 1599 (vs), 1582 (m), 1529 (s), 1488 (m), 1444 (s), 1387 (s). (Yield: 0.028 g,
157 28% on the basis of Yb).
158
159 2.5. X-ray crystal structures of 1–3 and 6
160 The X-ray diffraction data reveals that complexes 1–3 and 6 crystallize in the triclinic space group P 1.
161 In view of the similarity of the structures, only the one of compound 3 will be discussed as a
162 representative example.
163
164 2.6. [Gd2(l2-9-AC)4(9-AC)2(phen)2] (3) A labelled plot of the structure of the dinuclear compound 3 is
165 shown in Fig. 1a. Selected bond distances are listed in Table 1. The structure consists of a
166 centrosymmetric [Gd2(l2-9-AC)4(9-AC)2 (phen)2] dinuclear molecule in which each Gd(III) ion is
167 nine-coordinated. The coordination sphere GdN2O7 is formed by two N atoms from one chelating phen
168 ligand with Gd1–N1 and Gd1–N2 distances being 2.6353(14) and 2.5945(13) Å, respectively, two O
169 atoms from a chelating 9-AC ligand (Scheme 1c) with Gd1–O5 and Gd1–O6 distances of 2.4195(12) Å
170 and 2.4412(10) Å, respectively, and five O atoms from four 9-AC bridging ligands. These ligands
171 present two different kinds of coordination modes: the symmetrical syn, syn bridge (l2-g1:g1 or 2.11
172 using Harris notation) and the chelating-bridging (l2-g2:g1 or 2.21), represented in Scheme 1a and b,
173 respectively. For the syn, syn 9-AC bridging ligands the Gd1–O1 and Gd1–O20 bond distances are
174 2.3296(10) and 2.4075(12) Å, respectively. On the other hand, the chelating-bridging mode of 9-AC
175 ligands presents two different Gd1–O3 distances of 2.3340(11) and 2.5559(11) Å and a Gd1–O40 bond
176 length of 2.5825(13) Å with Gd1–O3–Gd10 angle of 106.40 (4) . The resultant Gd1···Gd10 (0: 1 x, 1

177 − y, 1 − z) intramolecular distance is 3.9177(4) Å and the shortest intermolecular Gd1− − − Gd10 (0:
178 − x, 1 − y, 1 − z) distance is 9.7275(6) Å (the intra- and intermolecular distances for compounds 1, 2
179 and 6 are collected in Table S2 of the Supplementary Information). The calculation of the degree of
180 distortion of the GdN2O7 coordination polyhedron for 3 (Fig. 1b) with respect to ideal nine-vertex
181 polyhedra, using the continuous shape measure theory and SHAPE software [36,37], shows intermediate
182 distortion between various coordination polyhedra. The lowest continuous shape measures (CShM's)
183 values for compound 3 correspond to spherical capped square antiprism (CSAPR-9), Muffin (MFF-9),
184 gyroelongated square pyramid J10 (JCSAPR-9) and tricapped trigonal prism (TCTPR-9) with values of
185 1.612, 1.759, 2.438 and 2.498, respectively. CShM's values for complexes 1–3 and 6 are listed in Table
186 S3 (Supplementary Section).
187 There are three different p-stacking supramolecular contacts between neighbouring dinuclear molecules;
188 one between two rings of two phenanthroline ligands that contain N1 (Cg(1) Table S4) in the [1 0 1]
189 direction of the network, another between the aromatic rings of the 9-AC carboxylate ligands in the
190 chelatingbridging coordination mode (Cg(6) and Cg(7) Table S4) in the [0 1 0] direction and the last
191 between two 9-AC in the chelating coordination mode (Cg(9) Table S4) in the [1 1 1] direction; these
192 contacts form a three-dimensional supramolecular structure. The network formed by the different
193 supramolecular contacts between [Gd2(l2-9-AC)4(9-AC)2(phen)2] dinuclear entities is shown in Fig. 2
194 and the intermolecular p-stacking parameters for compounds 1–3 and 6 are collected in Table S4.
195
196 2.7. Dc magnetic susceptibility studies
197 Static magnetic measurements were collected on polycrystalline powder samples of complexes 1–6 in
198 the temperature range of 2–300 K under applied fields of 0.3 T (for 1, 3–6) and 0.5 T (2). The data for
199 1–6 are plotted as vMT versus T in Fig. 3a. Room temperature vMT values for 1–6 are 3.27, 2.90, 16.13,
200 24.75, 22.39 and 6.11 cm3 mol− 1 K, respectively. The expected values for two isolated Ln(III) ions are
201 [38]: Nd(III) ground state 4I9/2 and gJ = 8/11, vMTcalc = 3.28 cm3 mol− 1 K; Eu(III) ground state 7F0
202 and vMTcalc = 0 cm3 mol− 1 K; Gd(III) ground state 8S7/2, gJ = 2, vMTcalc = 15.75 cm3 mol− 1 K;
203 Tb(III) ground state 7F6, gJ = 3/2, vMTcalc = 23.64 cm3 mol− 1 K; Er(III) ground state 4I15/2, gJ =
204 6/5, vMTcalc = 22.96 cm3 mol− 1 K; Yb(III) ground state 2F7/2, gJ = 8.7, vMTcalc = 5.14 cm3 mol− 1
205 K. The experimental vMT values are in good agreement with the calculated ones, except for compound
206 2. Although the magnetic ground state of Eu(III) is 7F0 a non-zero experimental value of vMT − 2.90
207 cm3 mol− 1 K is observed because of the second order effect due to Zeeman induced mixing of the close
208 lying excited state in the ground state [39]. Upon cooling, different behaviours are observed for the
209 different compounds. For 1, 2 and 6 the vMT values slightly decrease mainly due to the thermal
210 depopulation of the Stark sublevels combined with a significant magnetic anisotropy [40]. At 2.0 K, the
211 vMT values are 1.28, 0.04 and 4.98 cm3 mol− 1 K for 1, 2 and 6, respectively, indicating an mJ = 0
212 ground sublevel for Eu(III) ion (7F0). For 3, the vMT product remains almost constant until T = 20 K
213 and then drops down to 12.62 cm3 mol− 1 K at 2 K. Since Gd(III) has no orbital angular momentum

contribution, it is not affected by the spin–orbit coupling [41]. Therefore, the exchange interaction between the two Gd(III) ions from the molecule can be described by the Heisenberg–Dirac–Van Vleck (HDVV) spin Hamiltonian [42]:

$$H = -JS_1S_2 \quad (1)$$

It is not possible to apply Eq. (1) to the other Ln(III) since they need much more complex models, based on explicit ligand field and spin–orbit parameters [43]. Fitting of the experimental vMT data for 3 reveals a weak antiferromagnetic exchange parameter J = − 0.03 cm− 1 with g = 2.02, which are in good agreement with previously reported values for other similar dinuclear Gd(III) compounds [20,44]. Compound 4 shows almost constant values of vMT until 13 K and then the curve slightly increases up to 26.70 cm3 mol− 1 K at 6 K. At lower temperatures the curve drops arriving to 24.11 cm3 - mol− 1 K at 2 K. This behaviour suggests a possible competition between ferromagnetic and antiferromagnetic interactions between the Tb(III) ions.

In the case of compound 5 the vMT values gradually decrease upon cooling. At 2 K the curve falls down to a vMT value of 9.00 cm3 mol− 1 K. As for compounds 1, 2 and 6, this behaviour is mainly a consequence of the thermal depopulation of low lying crystal-field states and the magnetic anisotropy of Er(III) ions and/or due to weak antiferromagnetic interactions between the ions.

Magnetization measurements of 1–6 at 2 K are depicted in Fig. 3b. The Gd(III) complex 3 shows a saturation value of 14.15 NlB under an applied field of 5 T, corresponding to the expected value for two weakly coupled Gd(III) ions (14 NlB) [45]. Also compounds 4 and 6 show saturation values of 10.78 and 4.9 NlB respectively under an applied field of 5 T. The magnetization in compounds 1, 2 and 5 increases with the field up to 2.63, 0.12 and 10.05 NlB, respectively, at the highest applied magnetic field (5 T) but without saturation, indicating again the presence of magnetic anisotropy and/or partially populated excited states.

2.8. Ac magnetic susceptibility studies

Dynamic magnetic studies on compounds 1 and 4–6 were performed in order to study if they present SMM behaviour. The measurements reveal that at zero static external magnetic field none of the complexes show out-of-phase (v00 M) signals of the ac susceptibility at frequencies up to 1488 Hz. This fact may indicate a low magnetic anisotropy or that at zero dc field the Quantum Tunneling of Magnetization (QTM) process dominates the magnetization relaxation time (s). The QTM process can be suppressed or partially suppressed at low temperatures when a static magnetic field is applied [45,40].

For 5 and 6 the frequency dependence of v00 M reveals temperature dependent peaks when a dc field of 0.1 T (5) or 0.15 T (6) is applied under a 4 10 4 T ac field oscillating at frequencies between 1–1488 Hz for 5 and 10–1488 Hz for 6 in the temperature range of 1.8–6 K for 5 and 2.8–5.2 K for 6 (Fig. 4a and d, respectively). The optimal dc fields of 0.1 T for 5 and 0.15 T for 6 were chosen by scanning v00 M versus T (2–10 K) at different frequencies and the first field in which v00 M presented a maximum was chosen.

Ac susceptibility frequency dependences of both v0 M and v00 M were analysed for 5 and 6 using the generalized Debye model [46]. In the representation of the correspondent Cole–Cole plots (Fig. 4b and e), estimated a values close to zero revealing that a single relaxation time is mainly involved in the system relaxation process in these compounds [47]. The relaxation parameters obtained from the best fit are summarized in Tables S5 and S6.

The temperature dependence of the relaxation time (s) (Fig. 4c and f) shows that at temperatures above 2.4 K for 5 and 3.6 K for 6 the rate of s follows the Arrhenius law [s = s0 exp(Ueff/kBT)], leading to effective energy barriers of 5.2 and 20.9 cm 1 for 5 and 6, respectively, and pre-exponential factors (s0) of 1.05 10 5 s (5) and 4.7 10 7 s (6). These obtained relaxation values are in good agreement with other Er(III) and Yb(III) compounds with fieldinduced slow relaxation of the magnetisation found in the literature [40,48–50].

Nevertheless, the thermal dependences of s at low temperatures deviate from the linearity of the thermal Orbach process in both compounds. Therefore the relaxation rates at low temperatures were simulated using the expression s 1 = s0 1exp(Ueff/ kBT) + AT where the second term corresponds to the direct relaxation process (Fig. 4c and f). The best fit parameters are: s0 = 2.43 10 7 s, Ueff = 14.4 cm 1 and A = 1523 s 1 K 1 for complex 5 and s0 = 2.77 10 7 s, Ueff = 22.7 cm 1 and A = 33.21 s 1 K 1 for complex 6.

2.9. Photoluminescence studies

The emission properties of complexes 1–6 were studied at room temperature, at 77 K and at 10 K in the solid state. The excitation of the samples at 410 nm induces the luminescence of the Ln(III) ions emitting in the NIR, assigned to the 4F3/2?4IJ (J = 9/2, 11/2 and 13/2), 4I13/2?4I15/2 or 2F5/2?2F7/2 transitions for Nd(III), Er(III) and Yb(III), respectively but not the emission of Ln(III) ions that emit in the visible region. All complexes present residual emission of the ligand in the visible range between 400–500 nm, these spectra together with the excitation spectra can be found in the Supporting Information in Fig. S2.

2.10. Ligand-centred luminescence

Photophysical properties of complex 3 were performed in order to study the ligand-centred luminescence, as this complex presents the non-emissive Gd(III) centre. The room temperature emission spectrum (Fig. 5, in black) shows a broad emission between 425 and 620 nm with a maximum at 494 nm

(20243 cm 1). The spectrum recorded at 77 K (Fig. 5, in red) also presents a broad band between 450 and 620 nm with a maximum at 513 nm (19493 cm 1). The low-lying energy of the triplet state prevents the sensitization of the Tb(III) and Eu(III) complexes but it is compatible with the sensitization of NIR emitters like Nd(III), Er(III) and Yb(III).

2.11. Nd(III)-centred luminescence

Complex 1 shows the characteristic Nd(III) emission profile with three main transitions (Fig. 6 left, black line) 4F3/2?4I9/2 at 860 nm, 4F3/2?4I11/2 at 1070 nm, and 4F3/2?4I13/2 at 1300 nm. Cooling down to 77 K (Fig. 6 left, red line) strongly increases the resolution of the spectrum which allowed us to record in detail the first transition (4F3/2?4I9/2) and as it can be seen in Fig. 6 right, this emission presents five peaks which correspond to the five expected Stark levels for a J = 9/2 in low symmetry [55] centred at 875, 888, 895, 903, and 908 nm. This transition gives us information of the crystal field energy diagram of the neodymium ions in complex 1 and allows us to estimate the energy between the ground and the first excited mJ states of the fundamental 4I9/2 level, of about 150 cm 1. The difference between this value and the effective energy barrier value obtained from the Arrhenius fit of the ac data (8.0 cm 1) confirms that relaxation of the magnetization takes place by direct and/or Raman processes instead of a pure Orbach one [16].

2.12. Er(III)-centred luminescence

Complex 5 presents a main transition that corresponds to the 4I13/2?4I15/2 transition with its maximum at 1535 nm (Fig. 7, black spectrum). Lowering the temperature down to 77 K (Fig. 7, red spectrum) does not allow us to increase enough the resolution to have access to the crystal field splitting.

2.13. Yb(III)-centred luminescence

Complex 6 shows the characteristic Yb(III) transition emission profile, with the main transition 2F5/2?2F7/2 at 980 nm (Fig. 8, black spectrum). When lowering the temperature to 77 K (Fig. 8, red line) the emission band splits into five bands, with the maxima at: 980, 1000, 1007, 1013, and 1027 nm. This number of contributions is higher than the degeneracy of the 2F7/2 ground state (Kramer's doublets), which has a maximum of four contributions. As the two Yb(III) ions are crystallographically identical the additional emission contributions cannot be explained by the presence of two Yb(III) ions in the complex. The presence of additional bands could thus be attributed to additional transitions coming from the second and/or third mJ states of the 2F5/2 multiplet state by analogy with previous studies by Ouahab et al. [51,52] and Auzel et al. [53] or vibrational contributions. This prevents us to establish a clear crystal field energy diagram for the complex.

3. CONCLUSIONS

Here we have presented the structural, magnetic and luminescence studies of four new homodinuclear lanthanide compounds based on the use of 9-anthracenecarboxylic acid (9-HAC) and 1,10-phenanthroline (phen) ligands with formula [Ln2(l2-9-AC)4(9-AC)2(phen)2] (Ln(III) = Nd (1), Eu (2), Gd (3) and Yb (6)). For the already published Tb (4) and Er (5) complexes, that had only been structurally characterised, we presented here the magnetic and luminescence studies.

The Nd (1), Er (5) and Yb (6) complexes display sensitisation of the corresponding f–f emission transitions in the NIR range due to the ligand absorption followed by energy transfer processes to the metal. In the previous published compounds with formula [Ln2(l2-9-AC)4(9-AC)2(bpy)2] (Ln = Nd, Er, and Yb) [27] the corresponding sensitisation of the f–f transitions in the NIR range was also observed.

The fitting of the vMT product versus T of Gd(III) (3) compound by the Heisenberg–Dirac–Van Vleck (HDVV) spin Hamiltonian reveals a weak antiferromagnetic interaction between the two Ln (III) within the dinuclear unit. Additionally, dynamic magnetic measurements reveal the field-induced slow relaxation of the magnetisation for compounds 5 and 6, with effective energy barriers (Ueff) of 14.4 and 22.7 cm 1 respectively, and a pre-exponential factor (s0) of 1.0 10 5 s (5) and 4.7 10 7 s (6). Thus, compounds Er (5) and Yb (6) present both field-induced slow relaxation of the magnetisation and luminescent properties and can be considered to be multifunctional complexes. Few examples of magnetic and luminescent homometallic dinuclear compounds containing Er(III) [26,27,54,55] or Yb(III) [26,27,56,57] ions can be found in the literature.

342 **ACKNOWLEDGEMENTS**

343

344 R.V., B.C., and S.S. acknowledge the financial support from Spanish Government Grant PGC2018-
345 094031-B-I00. S. S. acknowledges the financial support from ‘‘Obra Social de la Fundació Bancària La
346 Caixa” and ‘‘La Fundació Universitaria Agustí Pedro i Pons”. O .M. and S. S. acknowledge the ANR
347 (French National Research Agency) for financial support (granted collaborative project ANR-15-CE29-
348 0019).

349

REFERENCES

[1] X.F. Tan, J. Zhou, H.H. Zou, L. Fu, Q. Tang, Inorg. Chem. 56 (2017) 10361.

[2] H.-Y. Shen, W.-M. Wang, H.-L. Gao, J.-Z. Cui, RSC Adv. 6 (2016) 34165.

[3] S.G. Reis, M. Briganti, S. Soriano, G.P. Guedes, S. Calancea, C. Tiseanu, M.A. Novak, M.A. Del Águila-Sánchez, F. Totti, F. Lopez-Ortiz, M. Andruh, M.G.F. Vaz, Inorg. Chem. 55 (2016) 11676.

[4] R.A. Layfield, M. Murugesu (Eds.), Lanthanides and Actinides in Molecular Magnetism, Wiley-VCH Verlag GmbH & Co. KGaA, 2015.

[5] J.D. Rinehart, J.R. Long, Chem. Sci. 2 (2011) 2078.

[6] D. Aguilà, L.A. Barrios, V. Velasco, O. Roubeau, A. Repollés, P.J. Alonso, J. Sesé, S.J. Teat, F. Luis, G. Aromí, J. Am. Chem. Soc. 136 (2014) 14215.

[7] M. Affronte, J. Mater. Chem. 19 (2009) 1731.

[8] L. Bogani, W. Wernsdorfer, Nat. Mater. 7 (2008) 179.

[9] L. Sorace, C. Benelli, D. Gatteschi, Chem. Soc. Rev. 40 (2011) 3092.

[10] S.V. Eliseeva, J.-C.G. Bünzli, Chem. Soc. Rev. 39 (2010) 189.

[11] A. D'Aléo, F. Pointillart, L. Ouahab, C. Andraud, O. Maury, Coord. Chem. Rev. 256 (2012) 1604.

[12] W. Xu, T.K. Lee, B.-S. Moon, D. Zhou, H. Song, Y.-J. Kim, S.K. Kwak, P. Chen, D.-H. Kim, V.Y. Panchenko, Nanoscale 9 (2017) 9238.

[13] C.-H. Huang, Rare Earth Coordination Chemistry: Fundamentals and Applications, John Wiley & Sons Ltd, Singapore, 2010.

[14] A. Ouchi, Y. Suzuki, Y. Ohki, Y. Koizumi, Coord. Chem. Rev. 92 (1988) 29.

[15] A.K. Jassal, B.S. Sran, Y. Suffren, K. Bernot, F. Pointillart, O. Cador, G. Hundal, Dalton Trans. 47 (2018) 4722.

[16] A.K. Jassal, N. Aliaga-Alcalde, M. Corbella, D. Aravena, E. Ruiz, G. Hundal, Dalton Trans. 44 (2015).

[17] B. Branchi, P. Ceroni, V. Balzani, F.G. Klärner, F. Vögtle, Chem. Eur. J. 16 (2010) 6048.

[18] M.A. Palacios, S. Titos-Padilla, J. Ruiz, J.M. Herrera, S.J.A. Pope, E.K. Brechin, E. Colacio, Inorg. Chem. 53 (2014) 1465.

[19] A.J. Calahorro, I. Oyarzabal, B. Fernández, J.M. Seco, T. Tian, D. Fairen-Jimenez, E. Colacio, A. Rodríguez-Diéguez, Dalton Trans. 45 (2015) 591.

[20] N.C. Anastasiadis, D.A. Kalofolias, A. Philippidis, S. Tzani, C. Raptopoulou, V. Psycharis, C.J. Milios, A. Escuer, S.P. Perlepes, Dalton Trans. 44 (2015) 10200.

[21] Z. Chen, M. Fang, X. Kang, Y. Hou, B. Zhao, Dalton Trans. 45 (2016) 85.

[22] Y.L. Wang, C.B. Han, Y.Q. Zhang, Q.Y. Liu, C.M. Liu, S.G. Yin, Inorg. Chem. 55 (2016) 5578.

[23] L. Song, J. Gao, J. Mol. Struct. 1032 (2013) 207.

[24] B. Casanovas, F. Zinna, L. Di Bari, M.S. El Fallah, M. Font-Bardía, R. Vicente, Dalton Trans. 46 (2017).

[25] K.P. Carter, K.E. Thomas, S.J.A. Pope, R.J. Holmberg, R.J. Butcher, M. Murugesu, C.L. Cahill, Inorg. Chem. 55 (2016) 6902.

[26] B. Casanovas, M. Font-bardía, S. Speed, S. El, R. Vicente, Eur. J. Inorg. Chem. 2018 (2018) 1928.

[27] B. Casanovas, S. Speed, O. Maury, M.S. El Fallah, M. Font-Bardía, R. Vicente, Eur. J. Inorg. Chem. 2018 (2018) 3859.

[28] B. Casanovas, S. Speed, M.S. El Fallah, R. Vicente, M. Font-Bardía, F. Zinna, L. Di Bari, Dalton Trans. 48 (2019) 2059.

[29] J. Long, Y. Guari, R.A.S. Ferreira, L.D. Carlos, J. Larionova, Coord. Chem. Rev. 363 (2018) 57.

[30] X. Yi, K. Bernot, F. Pointillart, G. Poneti, G. Calvez, C. Daiguebonne, O. Guillou, R. Sessoli, Chem. Eur. J. 18 (2012) 11379.

[31] H. Chang-Bao, W. Yu-Ling, L. Qing-Yan, Chin. J. Struct. Chem. 36 (2017) 705.

[32] C.-S. Liu, L.-Q. Guo, L.-F. Yan, J.-J. Wang, Acta Crystallogr., Sect. C: Cryst. Struct. Commun. 64 (2008) m292.

[33] G.M. Sheldrick, Acta Crystallogr., Sect. A: Found. Crystallogr. A 64 (2008) 112.

[34] G.M. Sheldrick, Acta Crystallogr., Sect. C: Struct. Chem. C 71 (2015) 3.

[35] C.-S. Liu, L.-F. Yan, Z. Chang, J.-J. Wang, Acta Crystallogr., Sect. E: Struct. Reports Online 64 (2008) m15.

[36] S. Alvarez, P. Alemany, D. Casanova, J. Cirera, M. Llunell, D. Avnir, Chem. Soc. Rev. (2005) 1693.

[37] M. Llunell, D. Casanova, J. Cirera, P. Alemany, S. Alvarez, (2013).

[38] D.A. Atwood (Ed.), The Rare Earth Elements: Fundamentals and Applications, John Wiley & Sons Ltd, 2005.

[39] L.E. Ballentine, D. Griffiths, Am. J. Phys. 59 (1991) 1153.

[40] T.Q. Liu, P.F. Yan, F. Luan, Y.X. Li, J.W. Sun, C. Chen, F. Yang, H. Chen, X.Y. Zou, G. M. Li, SI_Inorg. Chem. 54 (2015) 221.

[41] Y.-L. Li, Q.-Y. Liu, C.-M. Liu, Y.-L. Wang, L. Chen, Aust. J. Chem. 68 (2015) 488.

[42] N.F. Chilton, R.P. Anderson, L.D. Turner, A. Soncini, K.S. Murray, J. Comput. Chem. 34 (2013) 1164.

[43] F. Cimpoesu, F. Dahan, S. Ladeira, M. Ferbinteanu, J.P. Costes, Inorg. Chem. 51 (2012) 11279.

[44] A. Rohde, W. Urland, Inorg. Chim. Acta 359 (2006) 2448.

[45] W.-H. Zhu, X. Xiong, C. Gao, S. Li, Y. Zhang, J. Wang, C. Zhang, A.K. Powell, S. Gao, Dalton Trans. 46 (2017) 14114.

[46] S.M.J. Aubin, Z. Sun, L. Pardi, J. Krzystek, K. Folting, L.-C. Brunel, A.L. Rheingold, G. Christou, D.N. Hendrickson, Inorg. Chem. 38 (1999) 5329.

[47] Y.-N. Guo, G.-F. Xu, Y. Guo, J. Tang, Dalton Trans. 40 (2011) 9953.

[48] A.J. Calahorro, I. Oyarzabal, B. Fernández, J.M. Seco, T. Tian, D. Fairen-Jimenez, E. Colacio, A. Rodríguez-Diéguez, Dalton Trans. 45 (2016) 591.

[49] J.J. Le Roy, S.I. Gorelsky, I. Korobkov, M. Murugesu, Organometallics 34 (2015) 1415.

[50] F. Pointillart, O. Cador, B. Le Guennic, L. Ouahab, Coord. Chem. Rev. 346 (2017) 150.

[51] G. Cosquer, F. Pointillart, B. Le Guennic, Y. Le Gal, S. Golhen, O. Cador, L. Ouahab, Inorg. Chem. 51 (2012) 8488.

[52] S. Speed, M. Feng, G. Fernandez, Garcia, F. Pointillart, B. Lefeuvre, F. Riobé, S. Golhen, B. Le, Guennic, F. Totti, Y. Guyot, O. Cador, O. Maury, L. Ouahab, Inorg. Chem. Front. 4 (2017) 604.

[53] P. Goldner, F. Pell, D. Meicheninb, F. Auzey, J. Lumin. 71 (1997) 137.

[54] J.H. Jia, Q.W. Li, Y.C. Chen, J.L. Liu, M.L. Tong, Coord. Chem. Rev. 378 (2019) 365.

[55] P. Martín-Ramos, L.C.J. Pereira, J.T. Coutinho, F. Koprowiak, H. Bolvin, V. Lavín, I.R. Martín, J. Martín-Gil, M.R. Silva, New J. Chem. 40 (2016) 8251.

[56] F. Pointillart, B. Le Guennic, S. Golhen, O. Cador, O. Maury, L. Ouahab, Chem. Commun. 49 (2013) 615.

[57] S.G. Dogaheh, H. Khanmohammadi, E.C. Sañ, New J. Chem. 41 (2017) 10101.

441 **Legends to figures**

442 **Figure. 1.** (a) Partially labelled plot of compound 3. Hydrogen atoms are omitted for clarity. (b)
443 Coordination polyhedron of the Gd(III) ions in compound 3.
444
445 **Scheme 1.** Representation of the different coordination modes of 9-AC.
446
447 **Figure.2** Supramolecular arrangement representation of compound 3. p-stacking interactions are
448 represented in blue. (Color online.)
449
450 **Figure.3** Left: vMT vs. T plots for compounds 1–6. Blue solid line represents the best fit for complex 3
451 (see text). Right: Field dependence of the magnetization plots for compounds 1–6. (Color online.)
452
453 **Figure.4** Frequency dependence of v00 M for 5 (a) and for 6 (d). Cole–Cole plot of compound 5 (b) and
454 6 (e). Solid lines represent the fitting using generalized Debye models. Magnetization relaxation time [ln
455 (s)] vs. T 1 for 5 (c) and for 6 (f). Solid lines represent the theoretical fittings (see text).
456
457 **Figure.5** Emission spectra of complex 3 at kex = 360 nm at room temperature (in black) and at 77 K (in
458 red) in solid state. (Color online.)
459
460 **Figure.6** Left: emission spectra of complex 1 at kex = 410 nm at room temperature (in black) and at 77
461 K (in red) in solid state. Right: zoom of the 4F3/2?4I9/2 transition. (Color online.)
462
463 **Figure.7** Emission spectra of complex 5 at kex = 410 nm at room temperature (in black) and at 77 K (in
464 red) in solid state. (Color online.)
465
466 **Figure.8** Emission spectra of complex 6 at kex = 410 nm at room temperature (in black) and at 77 K (in
467 red) in solid state. (Color online.)
468
469

FIGURE 1

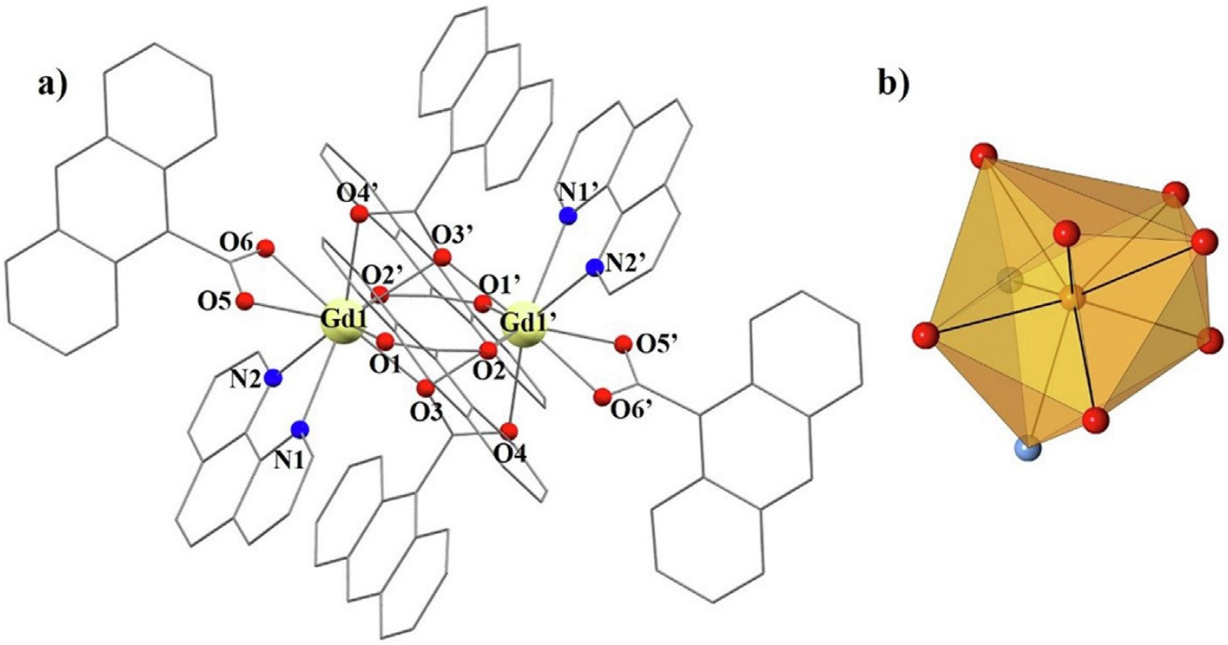

475 **SCHEME 1**

476

477

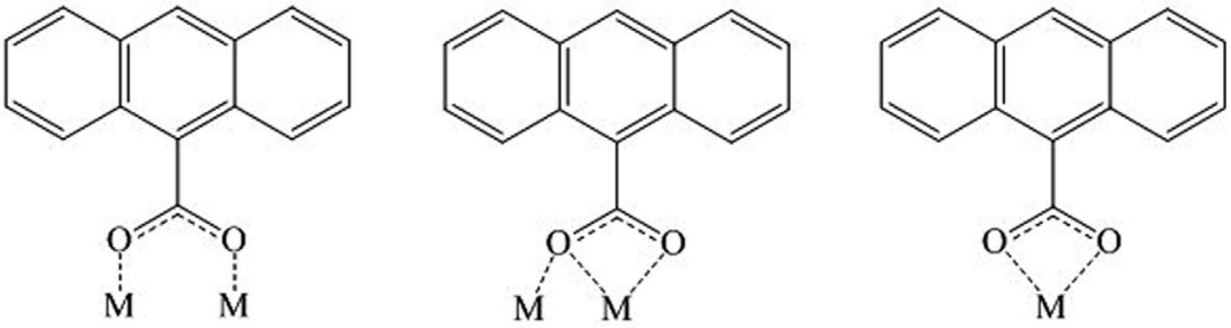

a) *syn, syn* bridge b) chelating-bridging c) chelating

478

479

480 **FIGURE 2**

481

482

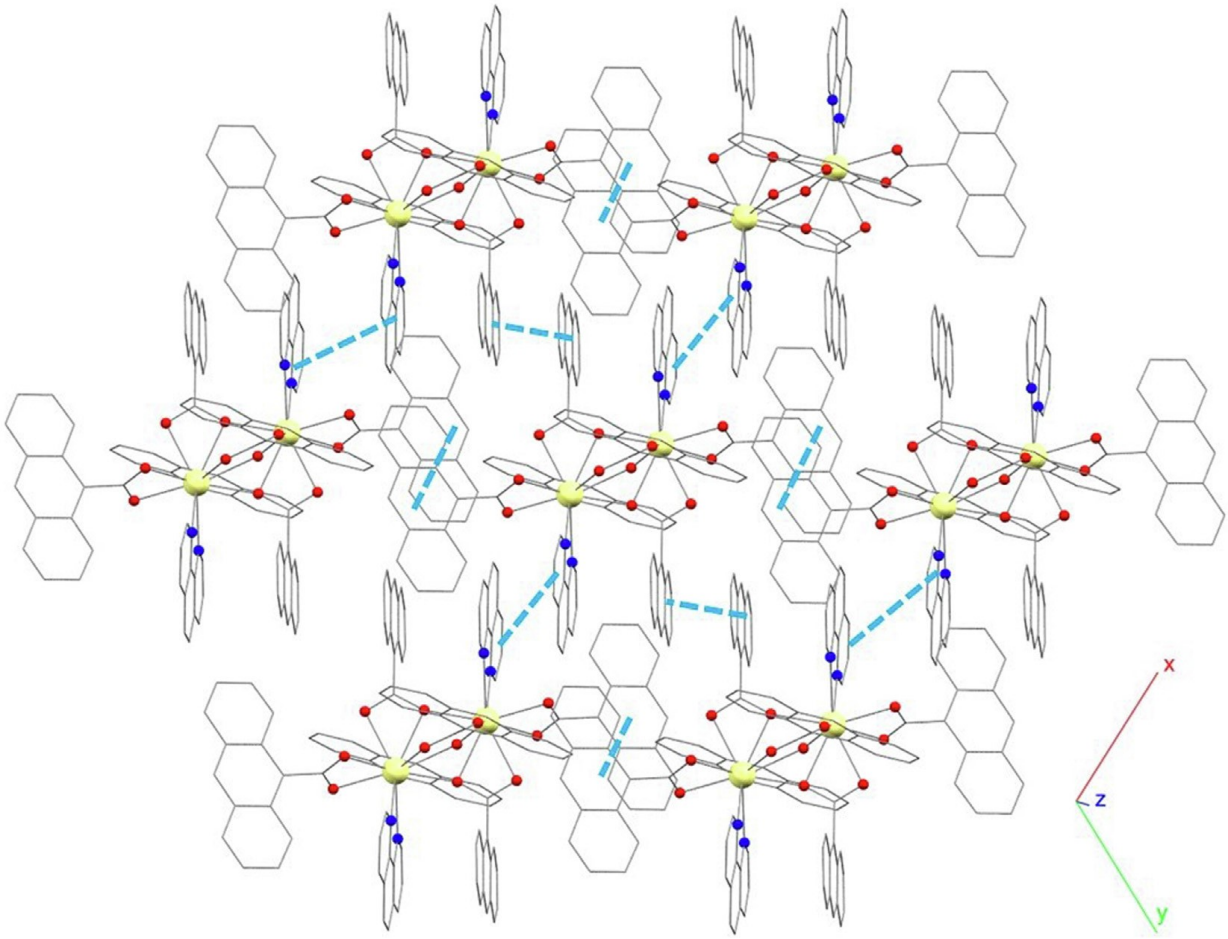

483

484

485 **FIGURE 3**

486

487

488

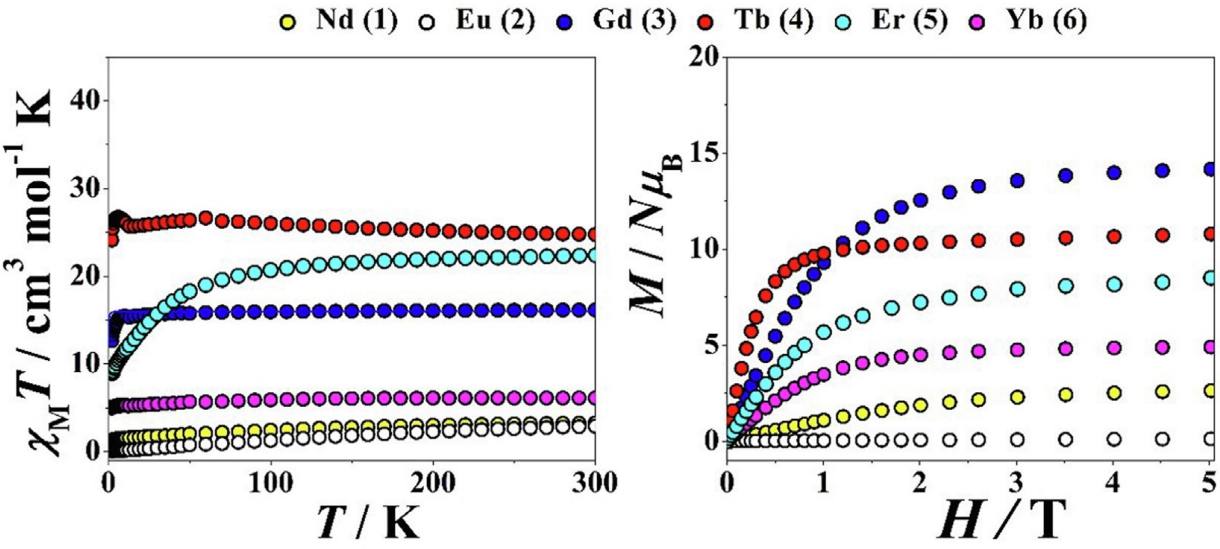

489

490

FIGURE 4

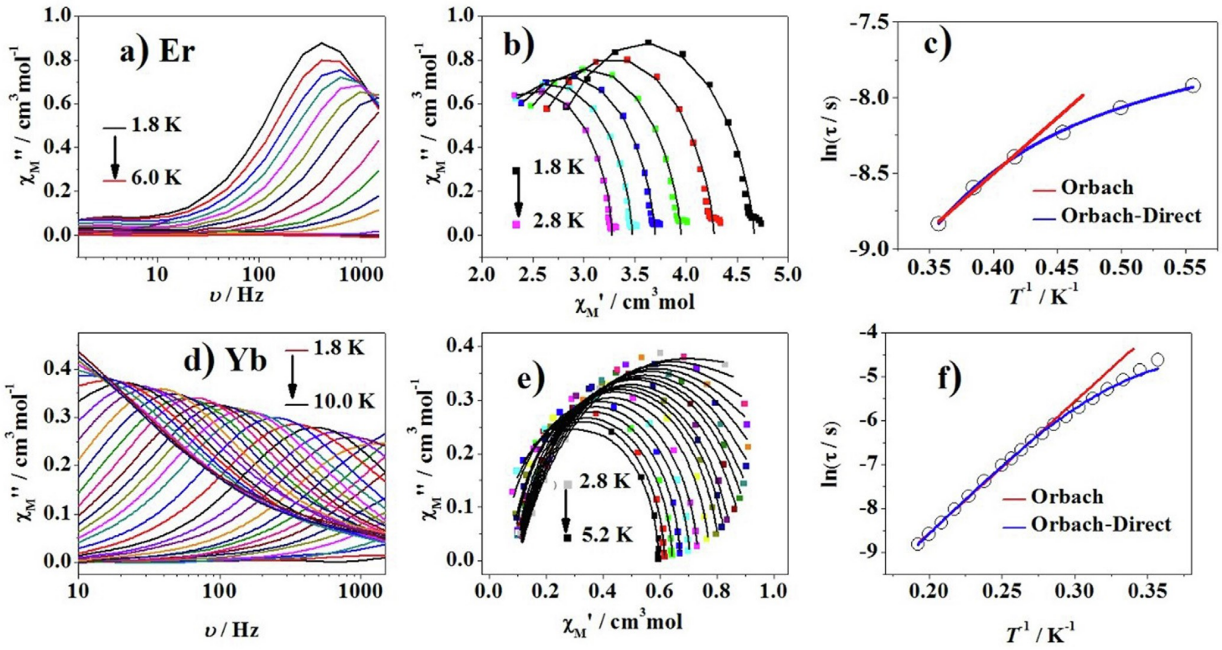
a) Er
1.8 K
6.0 K
χM'' / cm3mol-1
υ / Hz
b)
1.8 K
2.8 K
χM'' / cm3mol-1
χM' / cm3mol
c)
Orbach
Orbach-Direct
ln(τ / s)
T-1 / K-1
d) Yb
1.8 K
10.0 K
χM'' / cm3mol-1
υ / Hz
e)
2.8 K
5.2 K
χM'' / cm3mol-1
χM' / cm3mol
f)
Orbach
Orbach-Direct
ln(τ / s)
T-1 / K-1

FIGURE 5

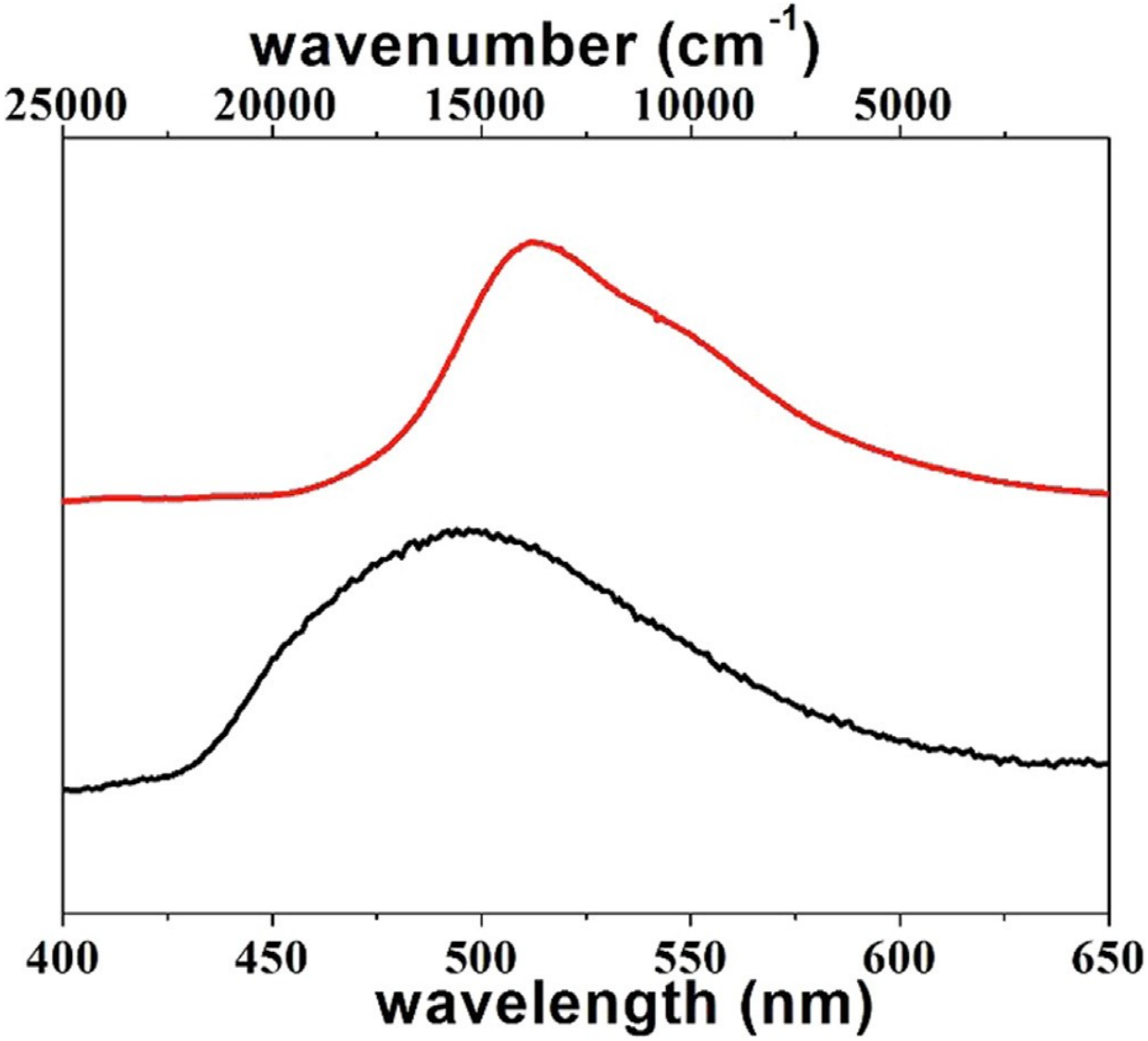
wavenumber (cm-1)
25000
20000
15000
10000
5000
400
450
500
550
600
650
wavelength (nm)

501 **FIGURE 6**

502

503

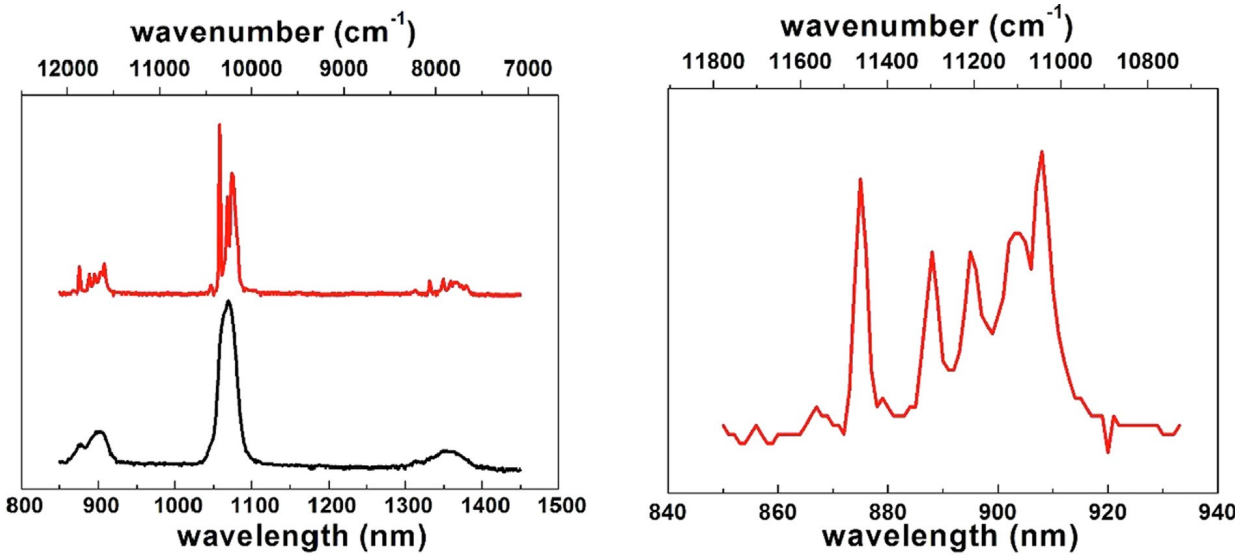

504

505

506 **FIGURE 7**

507

508

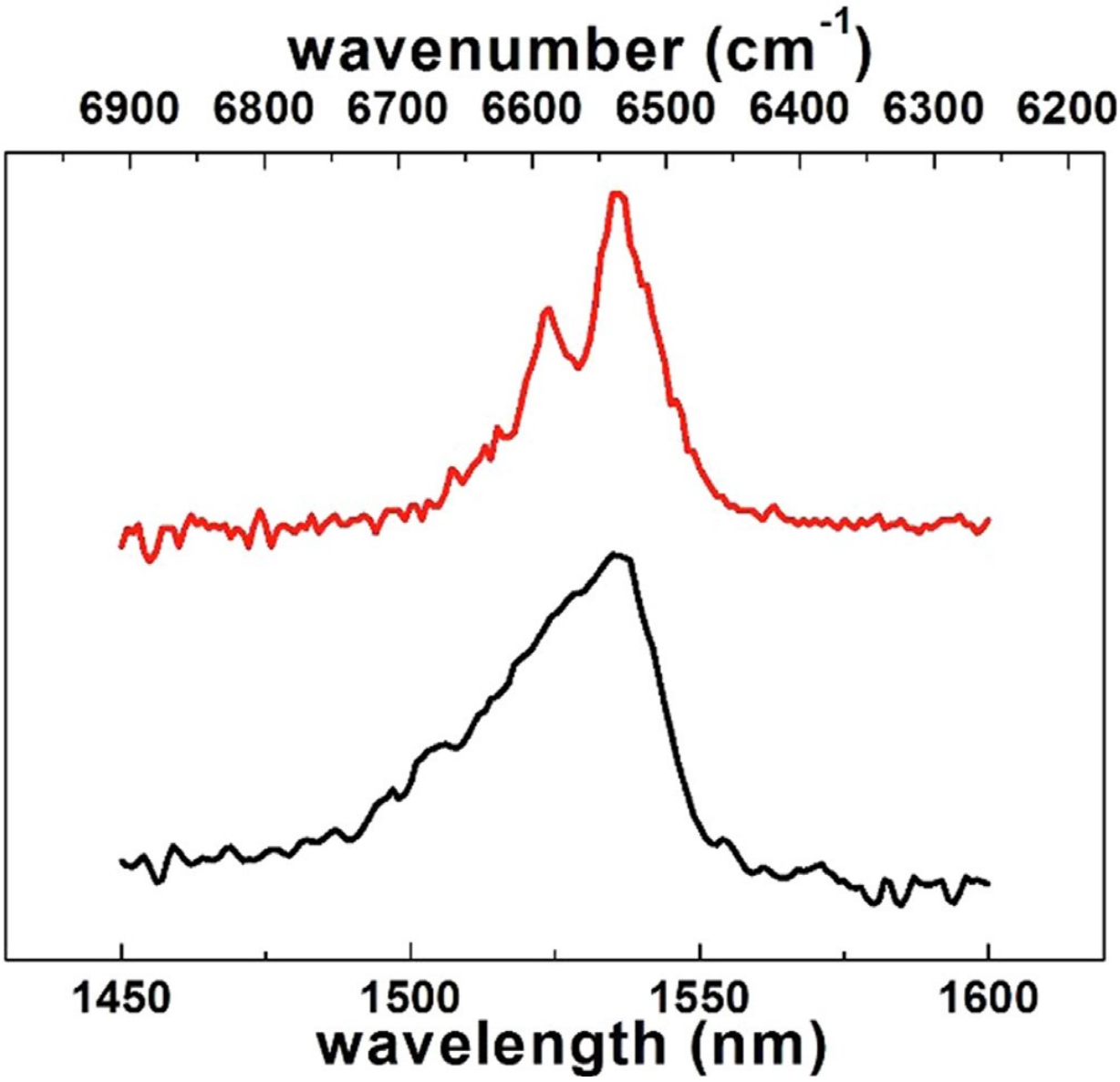

509

510 **FIGURE 8**

511

512

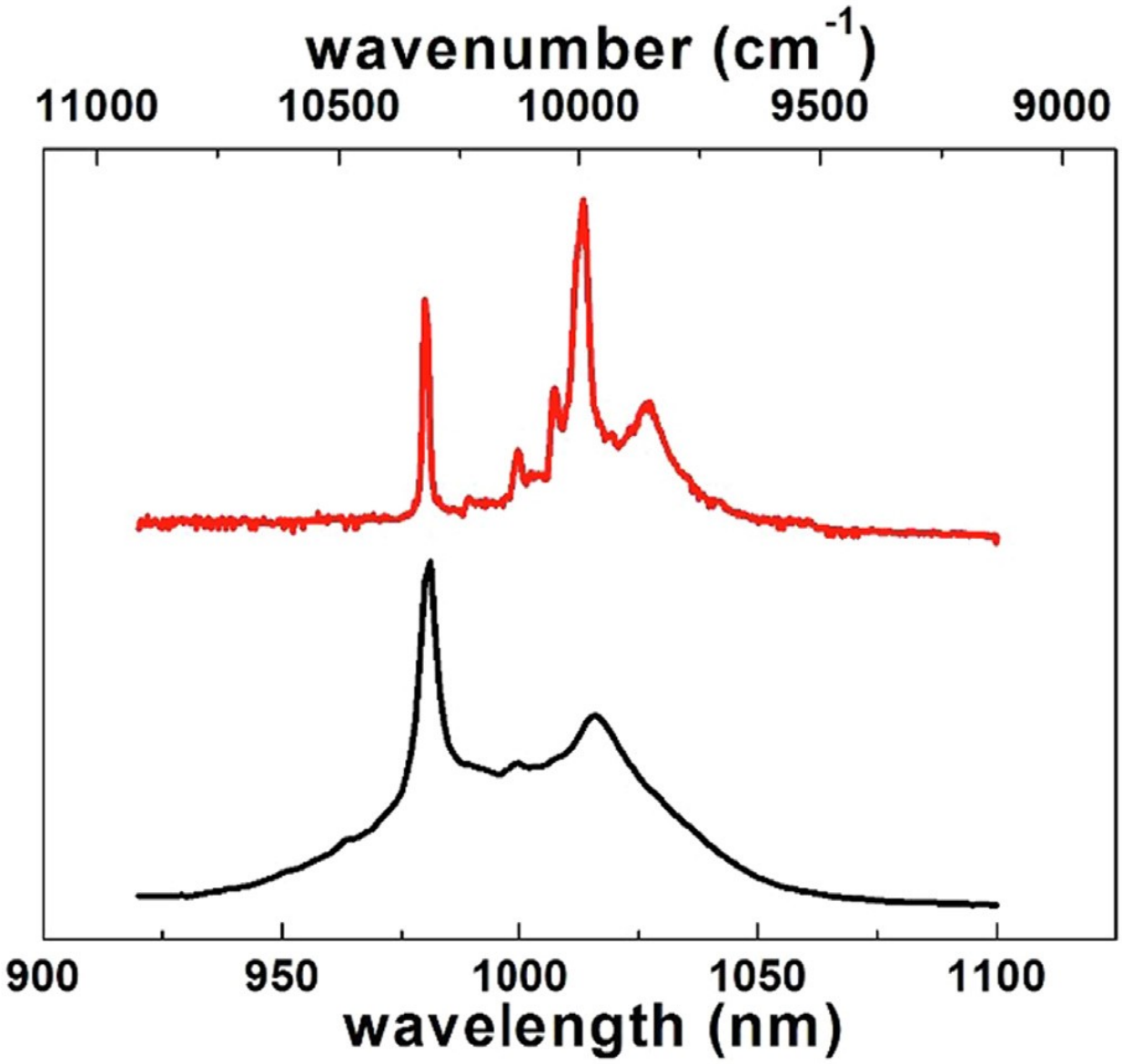

513

514

515 **Table 1** Selected bond distances (Å) for compounds 1–3 and 6.

516

Bond	1	2	3	6
Ln1—O1	2.3826(13)	2.3377(12)	2.3296(10)	2.244(3)
Ln1—O3	2.3921(13)	2.3446(13)	2.3340(11)	2.249(4)
Ln1—O5	2.4684(16)	2.4258(14)	2.4195(12)	2.347(4)
Ln1—O6	2.4778(13)	2.4455(11)	2.4412(10)	2.366(4)
Ln1—N1	2.6796(18)	2.6445(16)	2.6353(14)	2.579(5)
Ln1—N2	2.6495(16)	2.6045(16)	2.5945(13)	2.525(4)
Ln1—O2^{i}	2.4672(14)	2.4166(13)	2.4075(12)	2.333(4)
Ln1—O3^{i}	2.5836(15)	2.5591(13)	2.5559(11)	2.553(4)
Ln1—O4^{i}	2.6425(16)	2.5964(14)	2.5825(13)	2.519(4)
Ln1···Ln1^{i}	3.9792(4)	3.9268(4)	3.9177(4)	3.8504(10)
(^{i}) =	−x, 1 − y, 1 − z	−x, 1 − y, 1 − z	−x, 1 − y, 1 − z	2 − x, 1 − y, 1 − z

517